

# On the Composition of Earth's Short-Period Seismic Noise Field

by Keith D. Koper, Kevin Seats, and Harley Benz

**Abstract** In the classic microseismic band of 5–20 sec, seismic noise consists mainly of fundamental mode Rayleigh and Love waves; however, at shorter periods seismic noise also contains a significant amount of body-wave energy and higher mode surface waves. In this study we perform a global survey of Earth's short-period seismic noise field with the goal of quantifying the relative contributions of these propagation modes. We examined a year's worth of vertical component data from 18 seismic arrays of the International Monitoring System that were sited in a variety of geologic environments. The apertures of the arrays varied from 2 to 28 km, constraining the periods we analyzed to 0.25–2.5 sec. Using frequency-wavenumber analysis we identified the apparent velocity for each sample of noise and classified its mode of propagation. The dominant component was found to be  $L_g$ , occurring in about 50% of the noise windows. Because  $L_g$  does not propagate across ocean–continent boundaries, this energy is most likely created in shallow water areas near coastlines. The next most common component was  $P$ -wave energy, which accounted for about 28% of the noise windows. These were split between regional  $P$  waves ( $P_n/P_g$  at 6%), mantle bottoming  $P$  waves (14%), and core-sensitive waves ( $PKP$  at 8%). This energy is mostly generated in deep water away from coastlines, with a region of the North Pacific centered at 165° W and 40° N being especially prolific. The remainder of the energy arriving in the noise consisted of  $R_g$  waves (28%), a large fraction of which may have a cultural origin. Hence, in contrast to the classic microseismic band of 5–20 sec, at shorter periods fundamental mode Rayleigh waves are the least significant component.

*Online Material:* Distribution of noise slowness maxima for all IMS arrays.

## Introduction

It is well known that Earth's surface continuously vibrates in response to natural processes such as ocean waves and anthropogenic activities such as road traffic. Study of this ambient noise is a classic topic in seismology and has been ongoing for more than a century. At short periods ambient seismic noise can be used to estimate the shear velocity just beneath the surface (Okada, 2003), a quantity with important implications for seismic hazard. More recently, it has been shown that ambient seismic noise can be used to image deeply into Earth's crust (Sabra *et al.*, 2005; Shapiro *et al.*, 2005; O'Connell, 2007) and provide 4D monitoring of important geologic structures such as fault zones (Brenquier *et al.*, 2008a) and volcanoes (Brenquier *et al.*, 2008b). Consequently, there is strong interest in locating and characterizing sources of ambient seismic noise.

In this study, we carry out a global survey of Earth's short-period (0.25–2.5 sec) seismic noise field using arrays of the International Monitoring System (IMS). Arrays are beneficial for studying noise sources because they provide unambiguous information on the spectral content, direction,

and mode-type of the noise signal. At typical microseismic periods of 5–20 sec, seismic noise is dominated by fundamental mode Love and Rayleigh waves; however, at shorter periods there is a complicated mixture of fundamental mode surface waves, higher mode surface waves, and body waves (Bonnetfoy-Claudet *et al.*, 2006). Our primary goal in this article is to quantify the relative contributions of these propagation modes and document their geographic distribution.

The main difference between this article and previous work is the scope. Previous studies on the composition of seismic noise have generally used data from a single array or several arrays, and analyzed data on a time scale of weeks to months. Here we study noise from 18 arrays that vary in aperture over 2–28 km, have various array response functions, and are sited at a range of latitudes near passive and active margins and deep within continental interiors. Furthermore, we analyze the noise over a calendar year, accounting for seasonal variation in dominant noise sources. The main limitation of this article is that we analyze only vertical component seismograms, so we do not address Love waves and

other transverse energy that exists in the ambient seismic noise field.

### Overview of Previous Work

The two primary methods that have been used to study the structure of seismic noise are particle motion analysis and array analysis. Particle motion can indicate the direction of a microseismic source and distinguish between Love, Rayleigh, and body waves. Array analysis allows direct estimation of the 2D slowness vector and yields precise information on the apparent velocity and back azimuth. Especially for low amplitude energy, array analysis gives better directional constraints than particle motion analysis (Suteau-Henson, 1990; Harris, 1990), though the best characterization of the wavefield comes from combining the two approaches (e.g., Jurkevics, 1988). In the following paragraphs, we give an abridged review of the literature on the composition of seismic noise; for a comprehensive review, see Bonnefoy-Claudet *et al.* (2006).

#### Particle Motion Studies

One of the earliest particle motion studies of seismic noise was carried out in St. Louis, Missouri, in 1938 (Ramirez, 1940). Ramirez analyzed six months of data and found retrograde, elliptical particle motion at periods of 3–9 sec, indicating that Rayleigh waves were dominant. A later study analyzed 800 hours of microseism data with a dominant period of 5 sec recorded on a seismograph in Palisades, New York, over the years 1968–1971 (Rind and Donn, 1978, 1979). These authors observed both Rayleigh and Love waves, with the relative amplitude varying as a function of back azimuth. For most directions Rayleigh energy dominated, but for microseisms arriving from the northeast they estimated 60% of the energy consisted of Love waves.

Barstow *et al.* (1989) was one of the first studies to analyze the particle motion of seismic noise recorded on the seafloor. Using two samples of data from an ocean bottom seismometer deployed about 200 km west of San Francisco, these authors found spectral peaks near 3 sec, 7 sec, and 16 sec that had phase relations and amplitude ratios appropriate for fundamental mode Rayleigh waves. The most comprehensive particle motion study of ambient seismic noise was carried out by Tanimoto *et al.* (2006) in which they analyzed data recorded in 2000–2003 at approximately 70 stations in southern California. For about half of these stations, the vertical–radial phase differences at periods of 5–9 sec showed Rayleigh wave dominance; however, at shorter periods the phase differences were more ambiguous, implying the presence of Love and body waves.

#### Array Studies

Direct slowness observations of seismic noise did not become possible until the arrival of array seismology in the 1960s. Early studies with 1D arrays of seismometers

in boreholes gave evidence for the existence of higher mode Rayleigh waves (Douze, 1964) and *P* waves (Gupta, 1965; Seriff *et al.*, 1965) in seismic noise at periods less than 5 sec, though it was difficult to distinguish between the two. Using a 2D configuration Backus *et al.* (1964) analyzed noise recorded on a 19-element array in Tennessee with an aperture of about 4 km, and found phase velocities of 3.5–4.5 km/sec at periods of 0.2–1 sec, indicating the existence of higher mode Rayleigh waves. Using data from this same array and the Tonto Forest Observatory in Arizona, Backus (1966) observed apparent velocities of 16 km/sec and higher at periods of 1–2 sec, conclusively demonstrating the presence of teleseismic *P* waves in seismic noise.

An important step forward in studies of seismic noise became possible with the installation of the Large Aperture Seismic Array (LASA) in Montana in the late 1960s. At its height, LASA consisted of over 340 seismometers arranged in various subarrays with a maximum aperture of about 250 km. Several researchers took advantage of this unique facility to study ambient seismic noise (Toksoz and Lacoss, 1968; Lacoss *et al.*, 1969; Capon, 1969b; Haubrich and McCamy, 1969; Iyer and Healy, 1972; Cessaro and Chan, 1989). In general, they found a clear frequency dependence to the modal structure of the noise. At the longest periods of about 7–33 sec fundamental mode Rayleigh and Love waves were observed, but not body waves; at middle periods of about 3–7 sec a mix of higher mode Rayleigh waves (velocities around 3.5 km/sec) and teleseismic *P*-waves were observed; and at short periods of about 1–3 sec only teleseismic *P*-waves were observed. The higher mode Rayleigh energy came predominantly from the northeast, while the *P*-noise projected to deep water source regions in the Pacific and Atlantic, far from coastlines. The only exception was a study in which regional, rather than teleseismic, *P*-wave velocities were observed in the noise at LASA (Iyer and Healy, 1972); however, these authors analyzed only a single 1024-point sample of noise.

In Scandinavia, Bungum *et al.* (1971) reported a strongly anisotropic noise field at periods of 3–5 sec with power concentrated between 3 and 4 km/sec (indicative of higher mode Rayleigh waves) using a 12-element, 10-km aperture subarray of NORSAR. This study noted that the lack of body-wave energy was in contrast to the LASA studies, and speculated that it was because the NORSAR subarray was located near a coastline whereas LASA was located within a continent. A later, more comprehensive study of noise at NORSAR stated that fundamental mode Rayleigh and Love waves dominated the short- and long-period noise at NORSAR (Ringdahl and Bungum, 1977); a study of especially short-period noise at NORSAR found an organized propagating component down to a period of 0.125 sec with phase velocities mainly between 3 and 5 km/sec, which Bungum *et al.* (1985) interpreted as Rayleigh energy.

More recent array-based studies of noise have tended to focus on locating persistent sources of noise, though they still give some discussion of its composition. Friedrich *et al.*

(1998) analyzed four months of continuous noise recorded by the large-aperture Gräfenburg array (GRF) in Germany and smaller time segments of noise from the nearby ANISO experiment and from NORSAR. They analyzed data in the primary (12–20 sec) and secondary (6–11 sec) microseism bands and found mainly fundamental mode Love and Rayleigh waves, although they only considered observations that had surface wave phase velocities (2.5–4.3 km/sec). Interestingly, they found the ratio of Love to Rayleigh energy was different for the two microseism frequency bands, being about 6:5 for the primary band and 1:4 for the secondary band. Essen *et al.* (2003) analyzed two months of microseism data from four European arrays in a frequency band of 4–10 sec. For GRF they reported phase velocities of 3.0–3.5 km/sec, indicative of fundamental mode Rayleigh waves. Using vertical channels of the southern California ANZA array, Schulte-Pelkum *et al.* (2004) analyzed a three-week sample of noise and found phase velocities corresponding to Rayleigh waves (3.3 km/sec) in the pass band of 2–20 sec.

One of the clearest recent observations of body-wave energy in the secondary microseism band resulted from a 2006 analysis of seismic noise generated by Hurricane Katrina (Gerstoft *et al.*, 2006). Studying continuous seismic data recorded on about 150 southern California seismometers (at periods of 4–6 sec), these authors observed phase velocities of 11.7 km/sec, which is consistent with a regional distance *P*-waves turning in the upper mantle. Teleseismic *P* waves, and even core-sensitive *PKP* waves, have also recently been observed at periods of around 2 sec from the Chiang Mai array (CMAR) in Thailand (Koper and de Foy, 2008), at periods of 4–6 sec from the southern California seismic network (Gerstoft *et al.*, 2008), and at periods of

1–3 sec from the Yellowknife array (YKA) in Canada (Koper *et al.*, 2009). The latter study found that although a significant fraction of the YKA noise energy is in the form of teleseismic *P* waves, the dominant arrivals during most times of year were *L<sub>g</sub>* waves created by storms in the North Atlantic.

## Data and Methods

To carry out the noise survey we selected 18 IMS arrays that are sited in a wide variety of geologic environments (Fig. 1). Some arrays are located on stable cratons deep within the interior of continents, some are located in deforming continental lithosphere, and others are located near the coastlines of both active and passive margins. The main geographical bias is a lack of arrays in the southern hemisphere, especially South America, Africa, and Antarctica. The selected IMS arrays also have a wide variety of array responses. For example, although WRA and ASAR are located close to one another in central Australia, WRA is cross-shaped with an aperture of 26 km, while ASAR is circular with an aperture of 10 km. The aperture essentially determines the frequencies for which an array has reasonable slowness resolution, therefore these two arrays are complementary. The apertures of the IMS arrays we consider vary from 2 to 28 km (Fig. 2), constraining the range of periods we analyze to 0.25–2.5 sec (Table 1). For a fixed aperture, the particular arrangement of the array sensors affects the location of side lobes in slowness space, and the number of sensors affects the sharpness of the main lobe (e.g., Schweitzer *et al.*, 2002; Rost and Thomas, 2002).

For each array we requested a sample of data for every hour of every day from 1 January 2007 through 31 December 2007. Because seismic noise often varies seasonally, it is

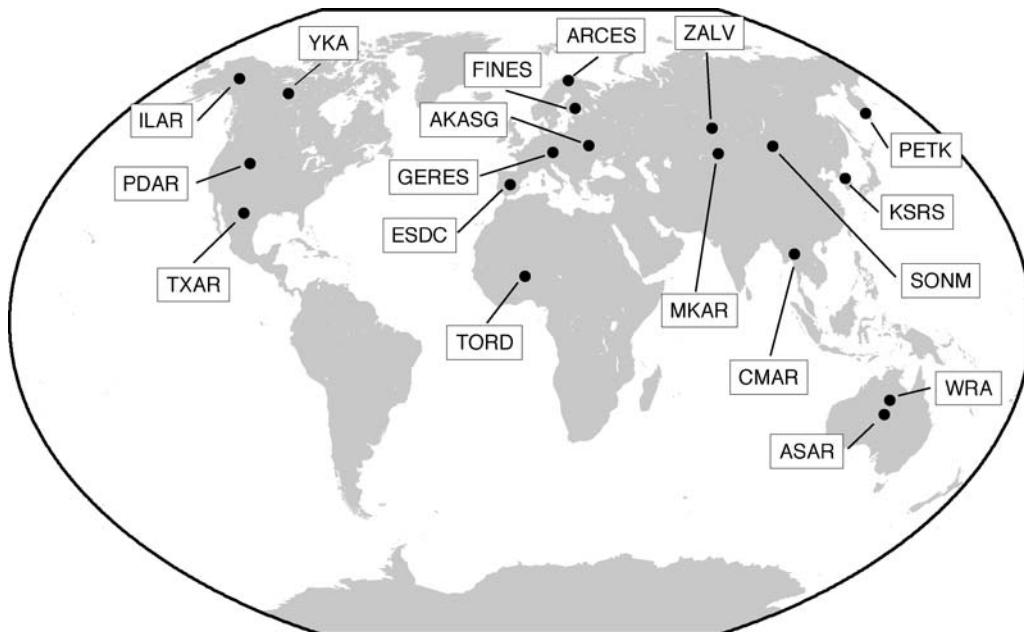


**Figure 1.** Locations and acronyms of IMS arrays used in this article.

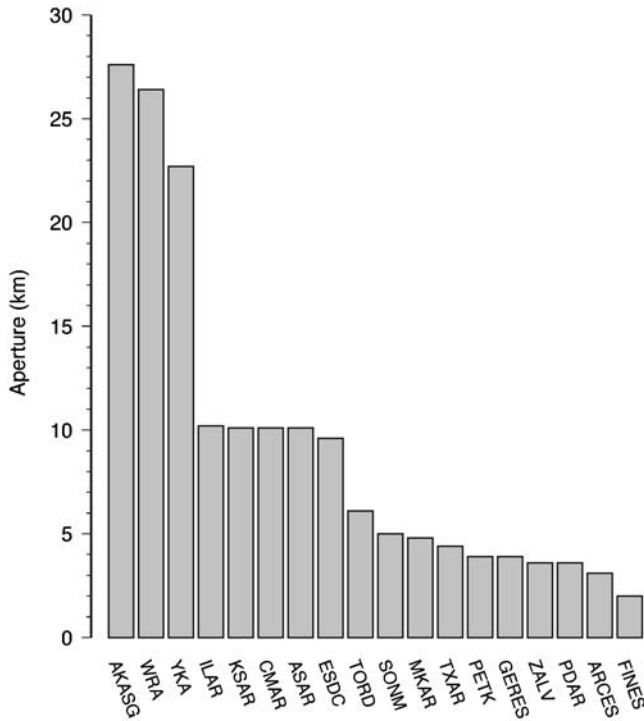


**Figure 2.** Apertures of arrays used in this article. Aperture is defined as the maximum interelement separation within an array.

important to observe its composition over an annual cycle. Each sample was five minutes long and started at a randomly selected time within the hour. Owing to various technical reasons usable data were not always returned and success rates varied between 40% and 85%. The specific number of samples used for each array are listed in Table 1; we emphasize that even for the array with the 40% return rate, there were still 3550 samples analyzed. Low success request rates primarily reflected data loss due to network communications

outages and/or downtime due to misconfiguration of the network support systems.

Our technique for estimating frequency-wavenumber ( $f$ - $k$ ) spectra was designed to average in both time and frequency, and is appropriate for diffuse, quasi-stationary signals such as coda waves or microseisms. Each noise sample was divided into  $M$  nonoverlapping subwindows, each  $N$  points long. The subwindows were individually detrended and tapered with a Hanning window. Spectral matrices were calculated for each subwindow by averaging over 11 discrete frequencies, and these in turn were averaged over the  $M$  subwindows. Each element of the matrix,  $S_{jl}$ , was then normalized by  $\sqrt{S_{jj}S_{ll}}$ ; the corresponding power spectrum was calculated across a uniform Cartesian slowness grid with bounds of  $\pm 50$  sec/deg and at increments of 0.5 sec/deg. The array specific processing parameters ( $M$ ,  $N$ , and frequency) are listed in Table 1.

The frequency bands analyzed for each array were carefully chosen to maximize slowness resolution while minimizing effects of spatial aliasing. For example, at the largest aperture array, AKASG, the station spacing is around 2 km, so the Nyquist wavenumber is about  $0.25 \text{ km}^{-1}$ . Therefore, we picked a center frequency of 0.51 Hz at which to calculate slowness spectra. Combined with the dimensions of slowness grid, this gives a maximum sampled wavenumber of about  $0.22 \text{ km}^{-1}$ , so aliasing is not a problem. This point is illustrated in Figure 3, in which we present the response of AKASG to a vertically incident plane wave for frequencies of 0.5 Hz and 1.0 Hz. At the higher frequency the main lobe of the response is sharper, indicating better slowness resolution; however, six prominent subpeaks appear at velocities between 3.0 km/sec and 4.0 km/sec. This sort of spatial aliasing could lead to confusion between teleseismic  $P$  waves and regional surface waves such as  $R_g$  or  $L_g$ , and is the reason we analyzed and interpreted noise at

Table 1  
Arrays Used in This Study

Array Name	Number of Elements	Aperture (km)	Number of Samples	$\Delta t$	Number of Points	Number of Windows	Frequency (Hz)
AKASG	24	27.6	7104	0.025	2048	5	$0.51 \pm 0.10$
ARCES	26	3.1	7386	0.025	1024	10	$3.98 \pm 0.19$
ASAR	19	10.1	7439	0.050	512	10	$1.02 \pm 0.19$
CMAR	18	10.1	7168	0.050	512	10	$1.02 \pm 0.19$
ESDC	20	9.6	7187	0.025	1024	10	$1.02 \pm 0.19$
FINES	16	2.0	5945	0.025	1024	10	$3.98 \pm 0.19$
GERES	25	3.9	7342	0.025	1024	10	$2.03 \pm 0.19$
ILAR	19	10.2	6770	0.050	512	10	$1.02 \pm 0.19$
KSRS	19	10.1	7136	0.050	512	10	$1.02 \pm 0.19$
MKAR	9	4.8	7295	0.025	1024	10	$1.52 \pm 0.19$
PDAR	13	3.6	7191	0.050	512	10	$2.03 \pm 0.19$
PETK	10	3.9	3550	0.025	1024	10	$2.03 \pm 0.19$
SONM	10	5.0	6979	0.020	1024	10	$1.51 \pm 0.24$
TORD	16	6.1	7272	0.025	1024	10	$1.52 \pm 0.19$
TXAR	9	4.4	7260	0.025	1024	10	$1.52 \pm 0.19$
WRA	24	26.4	6912	0.025	2048	5	$0.51 \pm 0.10$
YKA	18	22.7	6899	0.050	1024	5	$0.51 \pm 0.10$
ZALV	9	3.6	6941	0.025	1024	10	$2.03 \pm 0.19$

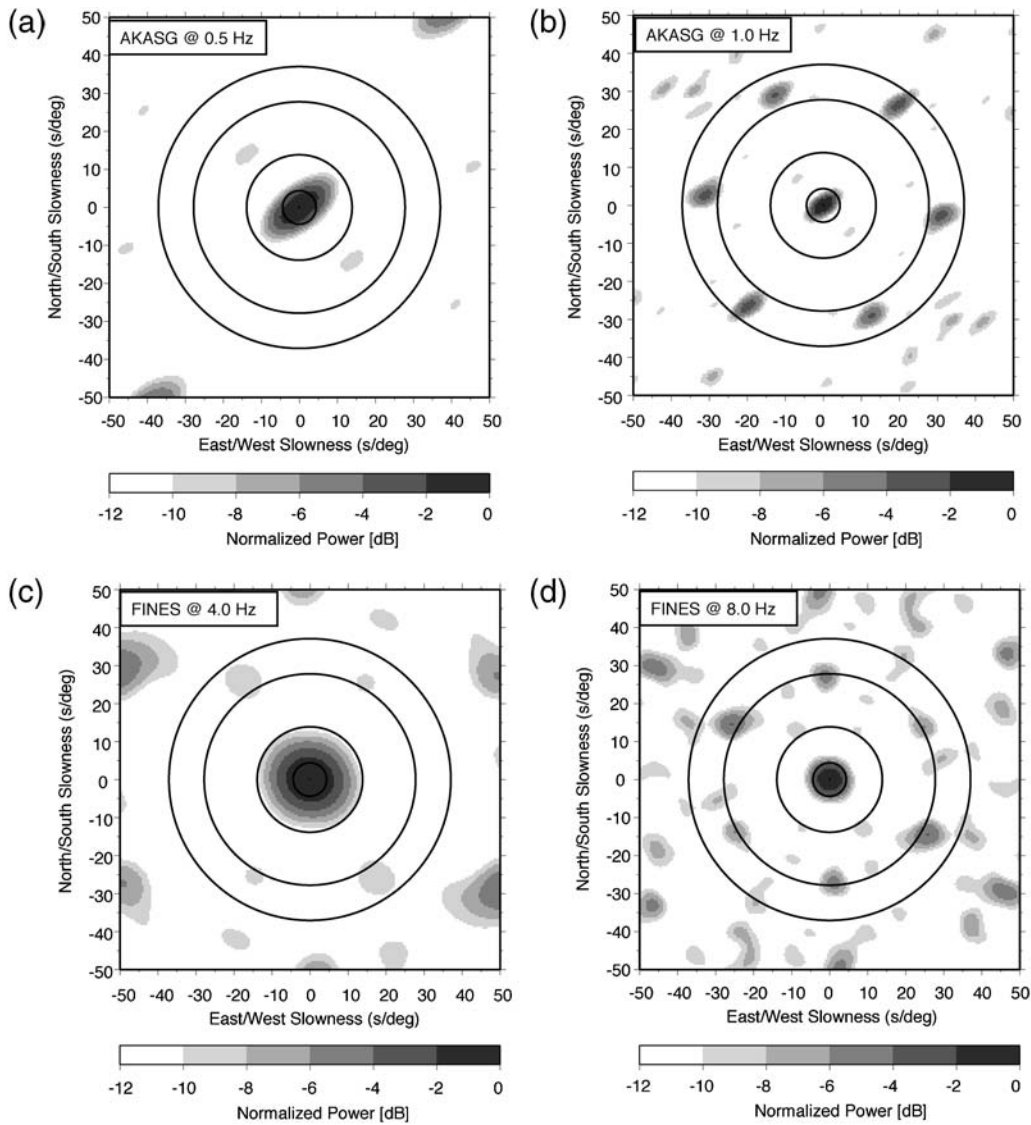


**Figure 3.** (a), (b) Array responses for AKASG at frequencies of 0.5 Hz and 1.0 Hz, and (c), (d) FINES at frequencies of 4.0 Hz and 8.0 Hz. In each panel, the circles are drawn at velocities of 3.0 km/sec ( $R_g$ ), 4.0 km/sec ( $L_g$ ), 8.0 km/sec ( $P_n$ ), and 25 km/sec ( $P_{diff}$ ). The ideal response would be a delta function at the origin, but because arrays are finite and discrete the response is smeared and side lobes appear. In order to mitigate the effect of spatial aliasing for both of these arrays we used the lower of the two frequencies shown.

AKASG near the lower frequency of 0.5 Hz. For comparison, in Figure 3 we also show the array response functions for the smallest aperture array (FINES) at the preferred frequency used in this article (4.0 Hz) and a larger frequency (8.0 Hz). The same trade-off between resolution and aliasing is evident.

Our method of f-k estimation is less sophisticated than other approaches. For instance, in a detailed study of noise at CMAR over a 10-year period, Koper and de Foy (2008) experimented with a time-domain method of f-k estimation based on the packing of beams created with phase weighted stacking. This nonlinear procedure produced spectra that were slightly sharper than classical frequency domain techniques, but the overall statistics of f-k maxima were no different. As a second example, in a study of noise recorded at

YKA over 17 years, Koper *et al.* (2009) found that conventional f-k estimation, as previously described, and the high-resolution approach suggested by Capon (1969a) gave similar results. Individual high-resolution spectra were sharper and possessed fewer artifacts; however, the statistical distributions of f-k maxima were not significantly different for the two approaches. Likewise, we feel that sophisticated multiplane wave approaches to f-k estimation (e.g., Goldstein and Archuleta, 1987; Shumway *et al.*, 2008) offer distinct advantages in cases where precise slowness estimates are required, for instance, when locating sparsely recorded seismic events, or perhaps when attempting to distinguish among triplicated, upper mantle  $P$  waves; however, they are unlikely to make a significant difference in the broad statistical analysis of noise that is the focus of this work.

### Results

To visualize the results of the f-k calculations we use histograms of slowness that correspond to global maxima on individual spectra. This approach provides a clearer image of consistent noise sources than 2D stacking of slowness grids. Smearing in the latter case is caused by noise sources having some geographic variability. Although this approach misses noise sources that are always smaller than a single dominant source, in our experience the relative power of noise sources varies considerably over a calendar year. Furthermore, by considering only the global maximum on a particular slowness grid, there is less of an impact from artificial local maxima that are created by the array response.

#### Detailed Analysis and Results for AKASG

Two-dimensional slowness histograms of the noise processed at each of the 18 arrays are presented in the electronic edition of *BSSA*. Shown in Figure 4 are the particular results for AKASG. This array has an aperture of 28 km and is located in the Ukraine, away from major coastlines. The 2D histogram of the 7104 slowness maxima is shown on the right and has four distinct clusters. The majority of noise arrives with a phase velocity around 4.0 km/sec, which is indicative of  $L_g$  waves (e.g., Kennett, 1986; Baumgardt, 1990). The  $L_g$  energy from the northwest is likely generated along the coastline of Norway, a region that is well known for

creating microseisms at periods of 5–10 sec (e.g., Essen *et al.*, 2003). Similarly, the  $L_g$  energy from the southeast is likely generated along the coastline of the Black Sea. Because  $L_g$  does not propagate across ocean–continent boundaries, it is unlikely that the energy is created in deep water regions. The sparse cluster of energy in the far southwestern quadrant is an artifact created by spatial aliasing of the dominant cluster to the northwest.

Perhaps more interesting are the two body-wave clusters shown in Figure 4 that lie inside of the 8 km/sec ring. One group arrives from the northwest with the most frequent slowness corresponding to a ray parameter of 8.1 sec/deg and a back azimuth of 300° N. Assuming this to be teleseismic  $P$  energy originating at the surface, it back projects to the North Atlantic, with the most frequent source location near 51° N and 43° W. This deep water area is well known for generating microseism energy via a nonlinear interaction between counterpropagating ocean waves (Kedar *et al.*, 2008). The other body-wave cluster arrives from the southwest with ray parameters smaller than 4.4 sec/deg, the value for  $P_{diff}$ . Therefore, this energy has interacted with Earth's core, most probably as  $PKP$  waves. Owing to the small  $dp/d\Delta$  values for  $PKP$  waves and the multiple branches that exist, it is difficult to back project this energy accurately. If we assume it consists of  $PKP_{BC}$  waves generated at the surface, this energy locates to the southern ocean, west of the Drake Passage. The most frequent source location is near 55° S and 105° W. This is

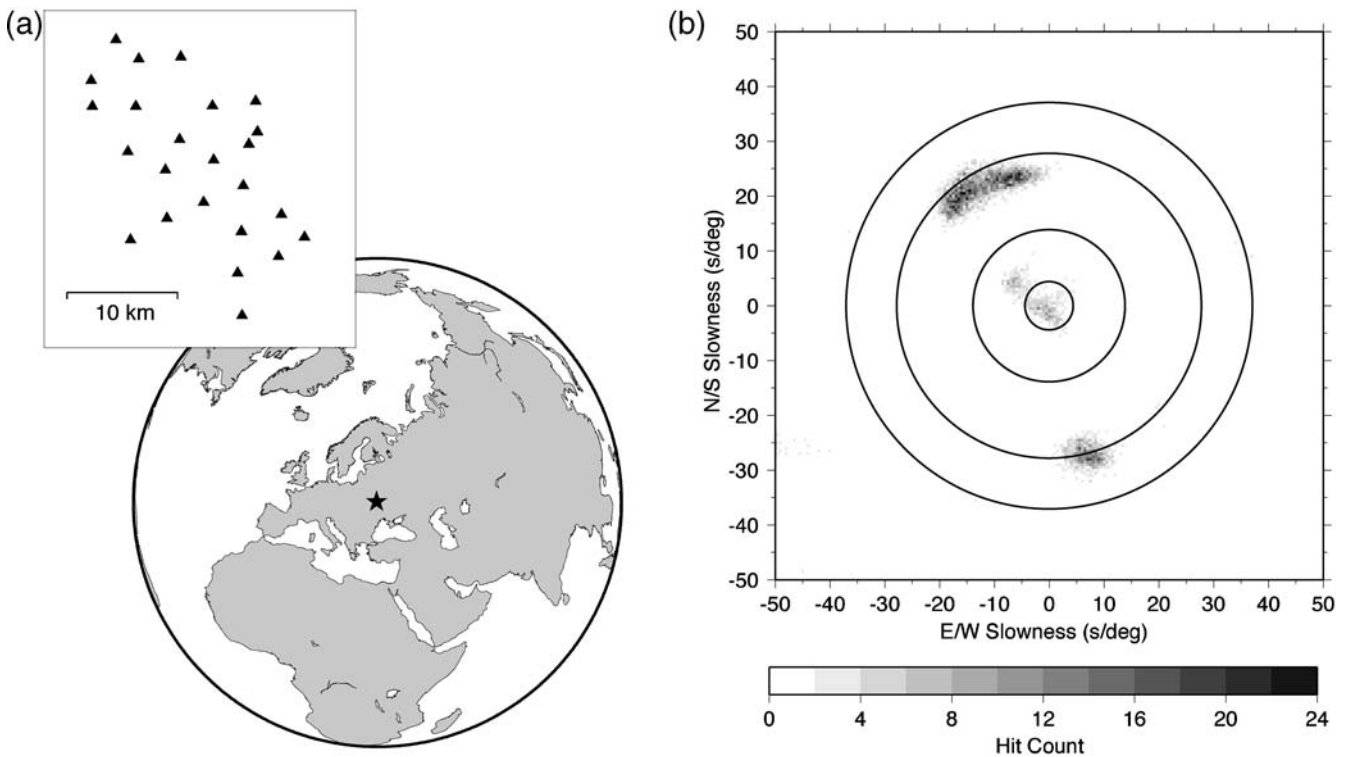


**Figure 4.** (a) The location and geometry of the AKASG array, and (b) a 2D histogram of the slowness maxima for the year 2007–2008. The circles in slowness space are drawn with radii of 4.4 sec/deg, 13.9 sec/deg, 27.8 sec/deg, and 37.1 sec/deg, corresponding to apparent velocities of  $P_{diff}$  (25 km/sec),  $P_n$  (8 km/sec),  $L_g$  (4 km/sec), and  $R_g$  (3.0 km/sec), respectively.

consistent with the work of [Koper and de Foy \(2008\)](#) who observed *PKP* energy from this direction at CMAR. [Koper and de Foy \(2008\)](#) found that the time dependence of the microseism energy was inconsistent with significant wave heights in the region. However, the energy should be expected to correspond to some measure of wave interference, and not necessarily significant wave height. In any case, an independent study of microseisms in southern California identified teleseismic body waves originating from this area in the southern ocean ([Gerstoft et al., 2008](#)).

In our analysis, we did not explicitly remove time windows that contained earthquake energy, so there is some contamination in the histogram presented in Figure 4. But because of the large number of time samples, the contamination is negligible. We illustrate this by considering the maximum normalized amplitude on the slowness grid for each time sample. This measure has a theoretical maximum of 1 for a perfectly coherent plane wave ([Capon, 1969a](#)). Figure 5 shows a plot of these values for all of the AKASG time windows. The relatively few earthquake waves in Figure 5 are apparent as large excursions away from the typical normalized amplitude value of about 0.15 for microseisms. We recalculated slowness histograms using only time samples with normalized amplitudes below certain thresholds and found the same results as shown in Figure 4. In fact, the four main clusters appear for a threshold as low as 0.125. Hence, the microseism analysis at AKASG is not biased by earthquakes or other sources of coherent seismic waves such as mining blasts.

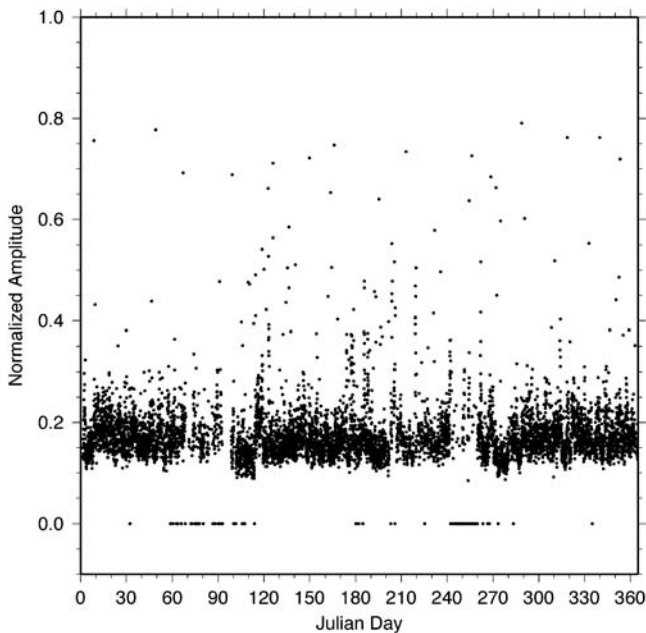


**Figure 5.** Maximum normalized amplitudes from the AKASG slowness grids. This metric reaches 1 for a perfectly coherent plane wave. The influence of earthquakes is indicated by values significantly higher than the microseism range of 0.1–0.3. A value of 0 is assigned to time windows for which no data were available.

## General Analysis and Results for All Arrays

To highlight the modal structure of the noise we binned the *f-k* maxima in fixed increments of scalar slowness (ray parameter). The corresponding histograms for each of the 18 IMS arrays are presented in Figures 6 and 7, ordered by decreasing aperture. To gauge the influence of earthquakes and mining blasts on these results, we recalculated the histograms using only those time windows in which the maximum normalized amplitude was less than the median of the entire population. In other words, for each array we eliminated the half of the time windows that had the most coherent waveforms. In all cases, the changes to the histograms were very subtle, and the positions and relative strengths of the peaks remained the same. As in the 2D slowness histogram for AKASG (Fig. 4), there is no bias from transient arrivals created by earthquakes or mining blasts in Figures 6 and 7. Instead, these slowness histograms reflect energy created by quasi-stationary natural processes such as ocean wave interactions and cultural activities such as traffic or construction.

Though each array has its own noise signature, some general trends are apparent. Many stations show two distinct peaks at the low phase velocities characteristic of surface waves (less than about 4.5 km/sec). These include YKA, CMAR, TORD, SONM, MKAR, GERES, ARCES, and FINES, and so span a wide range of aperture (i.e., frequency) and sample various geologic environments. The two peaks are separated by 1.0–1.5 km/sec in phase velocity. We attribute the bimodality to the existence of the two general types of surface waves observed on vertical component, short-period seismograms:  $R_g$  and  $L_g$ . The former are fundamental mode Rayleigh waves sensitive to the shallowest crust, and the latter are higher mode Rayleigh waves more sensitive to the lower crust (e.g., [He et al., 2008](#)). Hence,  $R_g$  phase velocities are distinctly lower than  $L_g$  velocities. The small variation in mean  $R_g$  and  $L_g$  velocities among the arrays can be explained by variations in local geology or perhaps site effects that bias the observed phase velocity away from the true phase velocity.

A more fundamental bimodality, between body waves and surface waves, is also evident at many of the arrays (e.g., AKASG, WRA, YKA, CMAR, ASAR, TORD, SONM, MKAR). The body-wave peaks have velocities significantly greater than 8.0 km/sec, consistent with teleseismic *P* waves; in some cases there are a significant number of arrivals with velocities above 25.0 km/sec, consistent with core-sensitive phases such as *PKP* (e.g., AKASG, YKA, CMAR, TORD, MKAR). In general, the region of slowness space in between surface waves and teleseismic body waves (velocities of about 4.5 km/sec to 8.0 km/sec) is nearly empty. This is the area that corresponds to local or regional *P* waves. The main exception is the PETK array in Kamchatka. Here the noise has a clear peak at a velocity near 5.8 km/sec, and a smaller shoulder at velocities around 8.0 km/sec, perhaps indicating the existence of  $P_g$  and  $P_n$  waves, respectively.

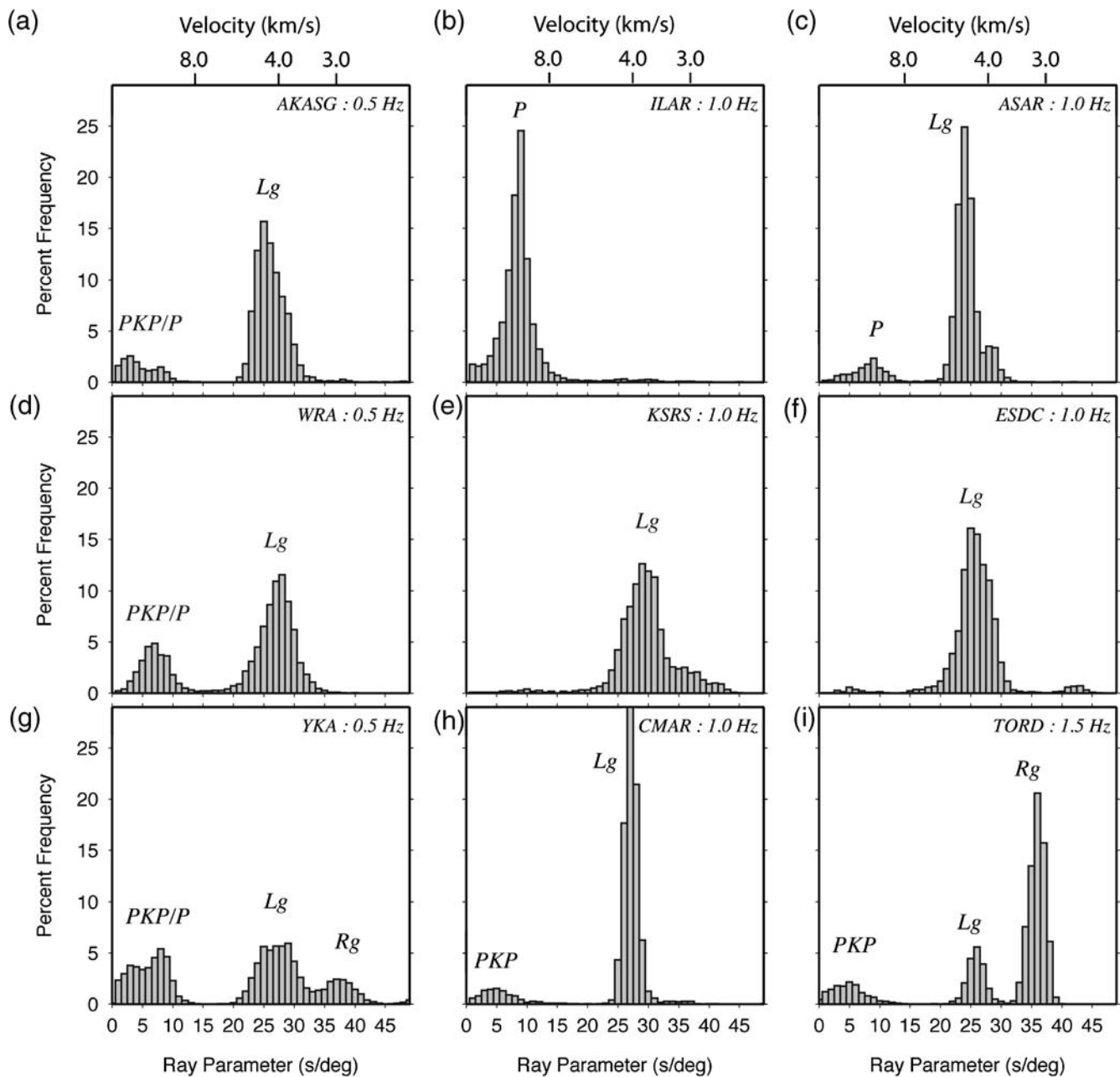


**Figure 6.** Histograms of apparent velocity for noise windows from nine of the IMS arrays with larger apertures.

Two arrays in North America show anomalous slowness distributions. The Pinedale, Wyoming, array (PDAR) possesses a single, robust peak in the surface wave band; however, the mean velocity is approximately 3.4 km/sec. Compared with the other arrays, this seems too low for  $L_g$  and too high for  $R_g$ . It might be explained by unusual 1D geologic conditions near the site, such as an abnormally low value for the sub-Moho  $S$  velocity that in turn creates an abnormally low upper bound on  $L_g$  phase velocity. Alternatively, the observations themselves may be biased by 3D site effects, such as intra-array variations in Moho depth. Previous work has found evidence for such slowness anomalies at PDAR (Bondar *et al.*, 1999). More anomalous is the slow-

ness distribution for the Lajitas, Texas, array (TXAR). Here the distribution is nearly flat, lacking both surface wave and body-wave peaks. Like PDAR, this array is known to possess significant site effects that bias slowness observations (Tibuleac and Herrin, 1997; Bondar *et al.*, 1999); however, it is unclear how this would lead to the appearance of an isotropic noise field.

#### The Persistent $P$ -Noise Source in the North Pacific

At most arrays the azimuthal distribution of arrivals is focused toward specific source regions, as shown in Figure 4 for AKASG. One persistent source of noise is strong enough

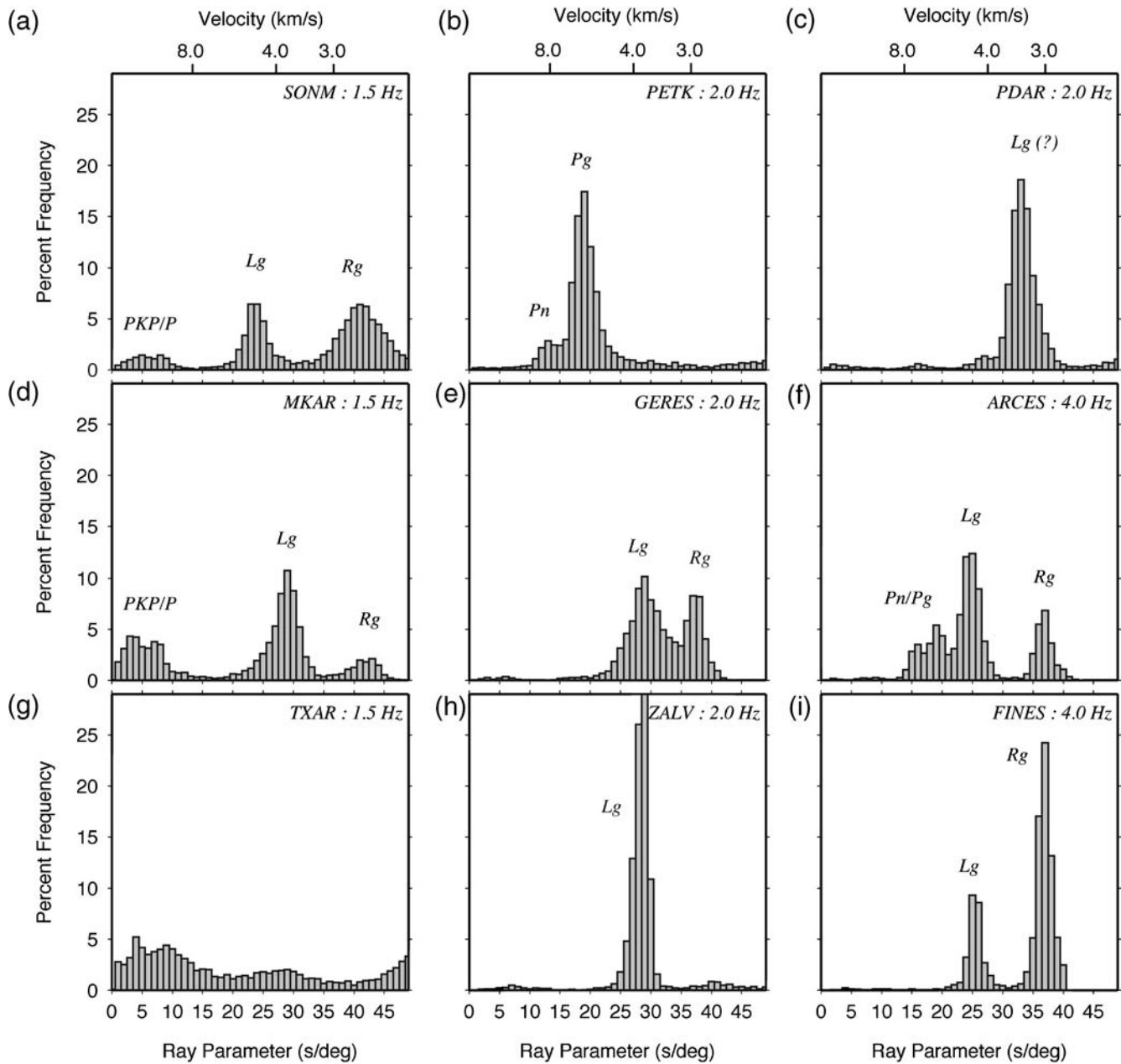


**Figure 7.** Histograms of apparent velocity for noise windows from nine of the IMS arrays with smaller apertures.

to be recorded by three array stations and so located to the intersection of the back azimuth estimates. We illustrate this in Figure 8, where we back project the  $P$  energy observed at PETK, ILAR, and YKA (see Figs. S3, S4, and S13 in the  $\text{\textcircled{E}}$  electronic edition of *BSSA*). The angular swaths intersect nicely for a patch of the North Pacific near  $165^\circ$  W and  $40^\circ$  N. For PETK the  $P$  waves are regional ( $P_g/P_n$ ) and do not constrain the distance to the source. For ILAR and YKA the  $P$  waves turn in the lower mantle and so can be projected to a range of distances. We note that these ranges do not include nearby coastlines. Instead, the projected distances are consistent with the patch defined by the intersection of back azimuth swaths.

## Discussion and Conclusions

Our global survey of the vertical component of Earth's short-period noise field shows that the most common mode of propagation is  $L_g$ . These waves make up almost 50% of all observations (Fig. 9).  $L_g$  waves are usually the most prominent arrivals on vertical component, short-period seismograms of earthquakes, so it is perhaps not surprising they also dominate on seismograms of noise.

At most arrays the  $L_g$  noise arrives from preferred directions that are oriented toward nearby coastlines (Figs. S1–S18 in the  $\text{\textcircled{E}}$  electronic edition of *BSSA*). The best example of this is the KSRS array located on the Korean peninsula

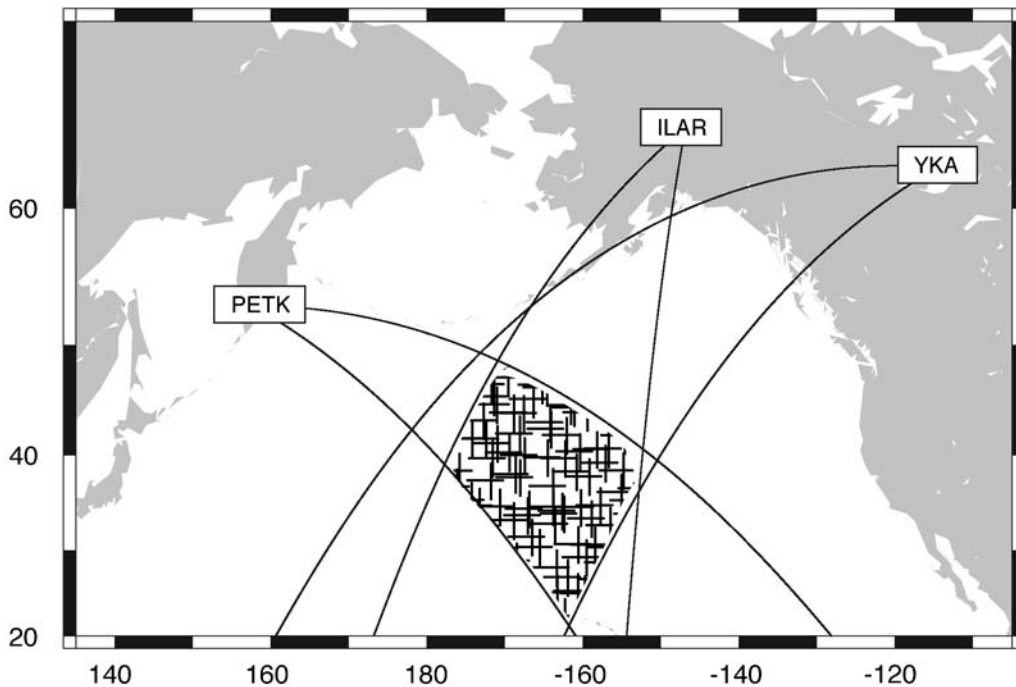


**Figure 8.** Back projection of  $P$  energy recorded in the noise from ILAR, YKA, and PETK using only back azimuth constraints. The  $P$  noise at PETK is regional and cannot be assigned a specific distance range, while distance ranges for the teleseismic  $P$  energy from ILAR and YKA are consistent with the hatched region shown.

(Fig. S5 in the  $\text{\textcircled{E}}$  electronic edition of *BSSA*). Here the  $L_g$  noise arrives from nearly all directions except for the north-west, which points toward the main Asian landmass. This implies that the  $L_g$  energy is being created by natural processes occurring in shallow, or near-coastal, oceanic regions. It is also consistent with previous long-term studies of noise at the IMS arrays of CMAR and YKA in which strong seasonal variations in  $L_g$  noise power were observed to correlate with the ocean wave climate (Koper and de Foy, 2008; Koper *et al.*, 2009).

The fact that  $L_g$  waves do not propagate in oceanic crust (e.g., Zhang and Lay, 1995) implies that this component of Earth's short-period noise field is created along shorelines of continental margins and not in the deep water regions of ocean basins. Presumably, the irregular morphology of many coastlines contributes to the generation of shear energy that then gets trapped in Earth's crust to appear as  $L_g$ . However, there have been observations of  $S_n$  waves created by oceanic earthquakes (Isacks and Stephens, 1975) and explosions (Baumgardt, 1990) converting into  $L_g$  at continental margins. Therefore, it is possible that in some cases the primary source of the seismic noise may be in the deep ocean, with the continental margins acting as a secondary, Huygen's type source of the  $L_g$  energy observed at IMS arrays.

Over 25% of the arrivals observed in the noise field are some type of  $P$  wave. The majority of these are  $P$  waves that turn in the mantle (14%), though a significant number of local ( $P_n/P_g$ , 6%) and core-sensitive ( $PKP$ , 8%) arrivals are recorded as well (Fig. 9). The body waves are recorded

across the full range of periods considered in this study, 0.25–2.5 sec, and in a variety of geographical locations. Therefore, compressional body-wave energy is a consistent

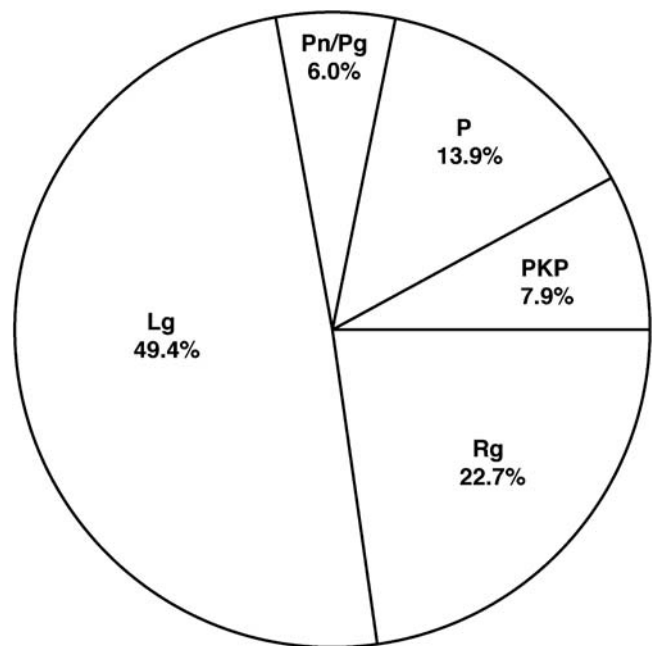


**Figure 9.** Phase distribution of noise from the 18 IMS arrays over the time period of 2007–2008. Apparent velocities used to separate the phases are:  $> 25$  km/sec for  $PKP$ , 25–8 km/sec for teleseismic  $P$ , 8–5 km/sec for regional  $P$ , 5–3.5 km/sec for  $L_g$ , and 3.5–2.5 km/sec for  $R_g$ .

and basic component of the short-period microseismic field. We were able to isolate one source region of  $P$  waves particularly well in the North Pacific. This region is far removed from coastlines and so is conclusive evidence for a pelagic source region. This area appears to be a stable, long-term generator of microseisms, having created  $P$  waves for at least the last 40 years (Anglin, 1971; Koper *et al.*, 2009).

Though it is currently debated whether the surface wave component of microseisms observed at continental sites is generated primarily along coastlines (Bromirski *et al.*, 1999; Bromirski, 2001; Bromirski *et al.*, 2005; Yang and Ritzwoller, 2008) or if it is also generated in deep-sea areas (Cessaro, 1994; Stehly *et al.*, 2006; Chevrot *et al.*, 2007; Kedar *et al.*, 2008), the work presented here and in other recent studies (Gerstoft *et al.*, 2006, 2008; Koper *et al.*, 2009) shows conclusively that teleseismic  $P$  waves are created in the open ocean in regions of deep water. The most likely source mechanism is that suggested by Longuet-Higgins, (1950) and simulated by Kedar *et al.* (2008) in which opposing trains of ocean waves interfere in a nonlinear manner to create a standing wave in which the pressure perturbation does not decay significantly as a function depth. This mechanism potentially operates at periods longer than those considered here, explaining the double-frequency band of microseisms at periods of about 5–10 sec, however, it can plausibly explain our observations as well. A similar interference mechanism was recently proposed to explain short-period, wind-induced microseismic energy at periods of 0.3 sec and shorter (Farrell and Munk, 2008).

The final propagation mode for seismic noise that was commonly observed in this study were fundamental mode Rayleigh waves ( $R_g$ ). In some cases, the  $R_g$  energy does not appear to originate from a nearby coastline and is likely cultural in origin (Fig. S9 in the  electronic edition of BSSA). Although the number of  $R_g$  observations are significant, accounting for just under a quarter of all observations, they were the least commonly observed type (Fig. 9). A possible explanation is that because of the relatively high attenuation of  $R_g$  energy, a receiver must be especially close by the source in order to record it. For instance, one source of  $R_g$  energy observed at YKA was estimated to have a  $Q$  of 45 (Weichert and Henger, 1976; Koper *et al.*, 2009). Nevertheless, it is important to keep in mind that  $R_g$  is still the least commonly observed component.

### Data and Resources

The seismograms used in this article were obtained from an internal server at the National Earthquake Information Center (NEIC); they are not accessible to the general public. For some arrays, equivalent data are available from the Incorporated Research Institutions for Seismology. The figures were made with the Generic Mapping Tools (GMT) of Wessel and Smith (1991).

### Acknowledgments

This work was partially supported by the U.S. Air Force Research Laboratory under contract FA871806C0003. During the writing of this article KDK was on sabbatical and hosted by the NEIC of the United States Geological Survey (USGS). Figure 2 was inspired by a similar figure produced by Neil Selby. We thank the following colleagues for critical comments on an earlier version of this article: Anton Dainty, Peter Gerstoft, Dan McNamara, Bill Stephenson, Jian Zhang, and an anonymous referee.

### References

- Anglin, F. M. (1971). Detection capabilities of the Yellowknife seismic array and regional seismicity, *Bull. Seismol. Soc. Am.* **61**, 993–1008.
- Backus, M. M. (1966). Teleseismic signal extraction, *Proc. R. Soc. A.* **290**, 343–367.
- Backus, M., J. Burg, D. Baldwin, and E. Bryan (1964). Wide-band extraction of mantle  $P$  waves from ambient noise, *Geophysics* **39**, 672–692.
- Barstow, N., G. H. Sutton, and J. A. Carter (1989). Particle motion and pressure relationships of ocean bottom noise: 3900 m depth; 0.003 to 0.05 Hz, *Geophys. Res. Lett.* **16**, 1185–1188.
- Baumgardt, D. R. (1990). Investigation of teleseismic  $Lg$  blockage and scattering using regional arrays, *Bull. Seismol. Soc. Am.* **80**, 2261–2281.
- Bondar, I., R. G. North, and G. Beall (1999). Teleseismic slowness-azimuth station corrections for the International Monitoring System seismic network, *Bull. Seismol. Soc. Am.* **89**, 989–1003.
- Bonnefoy-Claudet, S., F. Cotton, and P.-Y. Bard (2006). The nature of noise wavefield and its applications for site effects studies: A literature review, *Earth-Science Reviews* **79**, 205–227.
- Brenguier, F., M. Campillo, C. Hadziioannou, N. M. Shapiro, R. M. Nadeau, and E. Larose (2008). Postseismic relaxation along the San Andreas Fault at Parkfield from continuous seismological observations, *Science* **12**, 1478–1481.
- Brenguier, F., N. M. Shapiro, M. Campillo, V. Ferrazzini, Z. Duputel, O. Coutant, and A. Nercessian (2008). Towards forecasting volcanic eruptions using seismic noise, *Nature Geoscience* **1**, 126–130.
- Bromirski, P. D. (2001). Vibrations from the Perfect Storm, *G-cubed* **2**, no. 7, 1030.
- Bromirski, P. D., F. K. Duennbier, and R. A. Stephen (2005). Mid-ocean microseisms, *G-cubed* **6**, Q04009.
- Bromirski, P. D., R. E. Flick, and N. Graham (1999). Ocean wave height determined from inland seismometer data: Implications for investigating wave climate changes in NE Pacific, *J. Geophys. Res.* **104**, 20,753–20,766.
- Bungum, H., E. S. Huesbye, and F. Ringdal (1971). The NORSAR array and preliminary results of data analysis, *Geophys. J. R. Astr. Soc.* **25**, 115–126.
- Bungum, H., S. Mykkeltveit, and T. Kvaerna (1985). Seismic noise in Fennoscandia, with emphasis on high frequencies, *Bull. Seismol. Soc. Am.* **75**, 1489–1513.
- Capon, J. (1969a). High-resolution frequency-wavenumber spectrum analysis, *Proc. IEEE* **57**, 1408–1418.
- Capon, J. (1969b). Investigation of long-period noise at the Large Aperture Seismic Array, *J. Geophys. Res.* **74**, 3182–3194.
- Cessaro, R. K. (1994). Sources of primary and secondary microseisms, *Bull. Seismol. Soc. Am.* **84**, 142–148.
- Cessaro, R. K., and W. W. Chan (1989). Wide angle triangulation array study of simultaneous primary microseism sources, *J. Geophys. Res.* **94**, 15,555–15,563.
- Chevrot, S., M. Sylvander, S. Benahmed, C. Ponsolles, J. M. Lefevre, and D. Paradis (2007). Source locations of secondary microseisms in western Europe: Evidence for both coastal and pelagic sources, *J. Geophys. Res.* **112**, B11301.
- Douze, E. J. (1964). Rayleigh waves in short-period seismic noise, *Bull. Seismol. Soc. Am.* **54**, 1197–1212.

- Essen, H.-H., F. Kruger, T. Dahm, and I. Grevemeyer (2003). On the generation of secondary microseisms observed in northern and central Europe, *J. Geophys. Res.* **108**, 2506, doi [10.1029/2002JB002338](https://doi.org/10.1029/2002JB002338).
- Farrell, W. E., and W. Munk (2008). What do deep sea pressure fluctuations tell about short surface waves?, *Geophys. Res. Lett.* **35**, L19605, doi [10.1029/2008GL035008](https://doi.org/10.1029/2008GL035008).
- Friedrich, A., F. Kruger, and K. Klinge (1998). Ocean-generated microseismic noise located with the Gräfenberg array, *J. Seismol.* **2**, 47–64.
- Gerstoft, P., M. C. Fehler, and K. G. Sabra (2006). When Katrina hit California, *Geophys. Res. Lett.* **33**, L17308.
- Gerstoft, P., P. M. Shearer, N. Harmon, and J. Zhang (2008). Global *P*, *PP*, and *PKP* microseisms observed from distant storms, *Geophys. Res. Lett.* **35**, L23306.
- Goldstein, P., and R. Archuleta (1987). Array analysis of seismic signals, *Geophys. Res. Lett.* **14**, 13–16.
- Gupta, I. N. (1965). Standing-wave phenomena in short-period seismic noise, *Geophys. Res. Lett.* **30**, 1179–1186.
- Harris, D. (1990). Comparison of the direction estimation performance of high-frequency seismic arrays and three-component stations, *Bull. Seismol. Soc. Am.* **80**, 1951–1968.
- Haubrich, R. A., and K. McCamy (1969). Microseisms: Coastal and pelagic sources, *Rev. Geophys.* **7**, 539–571.
- He, Y., X.-B. Xie, and T. Lay (2008). Explosion-source energy partitioning and *Lg*-wave excitation: Contributions of free-surface scattering, *Bull. Seismol. Soc. Am.* **98**, 778–792.
- Isacks, B. L., and C. Stephens (1975). Conversion of *Sn* to *Lg* at a continental margin, *Bull. Seismol. Soc. Am.* **65**, 235–244.
- Iyer, H. M., and H. J. Healy (1972). Evidence for the existence of locally-generated body waves in the short-period noise at the Large Aperture Seismic Array, Montana, *Bull. Seismol. Soc. Am.* **62**, 13–29.
- Jurkevics, A. (1988). Polarization analysis of three-component array data, *Bull. Seismol. Soc. Am.* **78**, 1725–1743.
- Kedar, S., M. Longuet-Higgins, F. Webb, N. Graham, R. Clayton, and C. Jones (2008). The origin of deep ocean microseisms in the North Atlantic Ocean, *Proc. R. Soc. A* **464**, 777–793.
- Kennett, B. L. N. (1986). *Lg* waves and structural boundaries, *Bull. Seismol. Soc. Am.* **76**, 1133–1141.
- Koper, K. D., and B. de Foy (2008). Seasonal anisotropy in short-period seismic noise recorded in South Asia, *Bull. Seismol. Soc. Am.* **98**, 3033–3045.
- Koper, K. D., B. de Foy, and H. Benz (2009). Composition and variation of noise recorded at the Yellowstone Seismic Array, 1991–2007, *J. Geophys. Res.* **114**, B10310, doi [10.1029/2009JB006307](https://doi.org/10.1029/2009JB006307).
- Lacoss, R. T., E. Kelly, and M. N. Toksöz (1969). Estimation of seismic noise structure using arrays, *Geophysics* **34**, 21–38.
- Longuet-Higgins, M. (1950). A theory of the origin of microseisms, *Phil. Trans. R. Soc. Lond. A* **243**, 1–35.
- O'Connell, D. R. H. (2007). Concrete dams as seismic imaging sources, *Geophys. Res. Lett.* **34**, L20307, doi [10.1029/2007GL031219](https://doi.org/10.1029/2007GL031219).
- Okada, H. (2003). *The Microtremor Survey Method*, vol. 12 of Geophysical Monograph Series, Society of Exploration Geophysicists, Tulsa, Oklahoma.
- Ramirez, J. E. (1940). An experimental investigation of the nature and origin of microseisms at St. Louis, Missouri: Part two, *Bull. Seismol. Soc. Am.* **30**, 139–178.
- Rind, D., and W. L. Donn (1978). Microseisms at Palisades 1. Source location and propagation, *J. Geophys. Res.* **83**, 3525–3534.
- Rind, D., and W. L. Donn (1979). Microseisms at Palisades 2. Rayleigh wave and Love wave characteristics and the geologic control of propagation, *J. Geophys. Res.* **84**, 5632–5642.
- Ringdahl, F., and H. Bungum (1977). Noise level variation at NORSAR and its effect on detectability, *Bull. Seismol. Soc. Am.* **67**, 479–492.
- Rost, S., and T. Thomas (2002). Array seismology: Methods and applications, *Rev. Geophys.* **40**, doi [10.1029/2000RG000100](https://doi.org/10.1029/2000RG000100).
- Sabra, K. G., P. Gerstoft, P. Roux, W. A. Kuperman, and M. C. Fehler (2005). Surface wave tomography from microseisms in Southern California, *Geophys. Res. Lett.* **32**, doi [10.1029/2005GL023155](https://doi.org/10.1029/2005GL023155).
- Schulte-Pelkum, V., P. S. Earle, and F. L. Vernon (2004). Strong directivity of ocean-generated seismic noise, *G-cubed* **5**, Q03004, doi [10.1029/2003GC000520](https://doi.org/10.1029/2003GC000520).
- Schweitzer, J., J. Fyfe, S. Mykkeltveit, and T. Kvaerna (2002). Chapter 9: Seismic arrays, in *IASPEI New Manual of Seismological Observatory Practice*, P. Bormann (Editor), p. 55, GeoForschungsZentrum, Potsdam.
- Seriff, A. J., C. J. Velzeboer, and R. J. Haase (1965). Possible *P*-wave observations in short-period seismic noise, *Geophysics* **30**, 1187–1190.
- Shapiro, N. M., M. Campillo, L. Stehly, and M. H. Ritzwoller (2005). High-resolution surface-wave tomography from ambient seismic noise, *Science* **307**, 1615–1618.
- Shumway, R. H., E. Smart, and D. A. Clauter (2008). Mixed signal processing for regional and teleseismic arrays, *Bull. Seismol. Soc. Am.* **98**, 36–51.
- Stehly, L., M. Campillo, and N. M. Shapiro (2006). A study of the seismic noise from its long-range correlation properties, *J. Geophys. Res.* **111**, B10306, doi [10.1029/2005JB004237](https://doi.org/10.1029/2005JB004237).
- Suteau-Henson, A. (1990). Estimating azimuth and slowness from three-component and array stations, *Bull. Seismol. Soc. Am.* **80**, 1987–1998.
- Tanimoto, T., S. Ishimaru, and C. Alvizuri (2006). Seasonality in particle motion in microseisms, *Geophys. J. Int.* **166**, 253–266.
- Tibuleac, I., and E. Herrin (1997). Calibration studies at TXAR, *Seism. Res. Lett.* **68**, 353–365.
- Toksoz, M. N., and R. T. Lacoss (1968). Microseism: Mode structure and sources, *Science* **159**, 872–873.
- Weichert, D. H., and M. Henger (1976). The Canadian seismic array monitor processing system (CANSAM), *Bull. Seismol. Soc. Am.* **66**, 1381–1403.
- Wessel, P., and W. Smith (1991). Free software helps map and display data, *Eos Trans. AGU* **72**, 441, 445–446.
- Yang, Y., and M. H. Ritzwoller (2008). The characteristics of ambient seismic noise as a source for surface wave tomography, *G-cubed* **9**, no. 2, Q02008, doi [10.1029/2007GC001814](https://doi.org/10.1029/2007GC001814).
- Zhang, T.-R., and T. Lay (1995). Why the *Lg* phase does not traverse oceanic crust, *Bull. Seismol. Soc. Am.* **85**, 1665–1678.

Department of Earth and Atmospheric Sciences  
 Saint Louis University  
 3642 Lindell Blvd  
 St. Louis, Missouri 63108  
 koper@eas.slu.edu  
 (K.D.K., K.S.)

United States Geological Survey  
 Box 25046, MS966  
 Denver, Colorado 80225  
 (H.B.)